# Directed Self-Assembly of Densely Packed Gold Nanoparticles

**ARTICLE** *in* LANGMUIR · SEPTEMBER 2012

Impact Factor: 4.46 · DOI: 10.1021/la303287z · Source: PubMed



**7 AUTHORS**, INCLUDING:

Mohamed Asbahi
Agency for Science, Technology and Research …
**20** PUBLICATIONS **46** CITATIONS
SEE PROFILE

Joel K W Yang
Singapore University of Technology and Design
**106** PUBLICATIONS **3,023** CITATIONS
SEE PROFILE

Langmuir

Article

pubs.acs.org/Langmuir

# Directed Self-Assembly of Densely Packed Gold Nanoparticles

Mohamed Asbahi,[†] Kevin T. P. Lim,[†] Fuke Wang,[†] Huigao Duan,[†] Naganivetha Thiyagarajah,[‡] Vivian Ng,[‡] and Joel K. W. Yang*[,†]

[†]Institute of Materials Research and Engineering, Agency for Science, Technology and Research (A*STAR), 117602, Singapore

[‡]Information Storage Materials Laboratory, Department of Electrical and Computer Engineering, National University of Singapore, 117576, Singapore

Supporting Information

**ABSTRACT:** Directing the self-assembly of sub-10-nm nanoparticles has been challenging because of the simultaneous requirements to achieve a densely packed monolayer and rearrange nanoparticles to assemble within a template. We met both requirements by separating the processes into two steps by first forming a monolayer of gold nanoparticles on a suitable liquid subphase of anisole and then transferring it edgewise onto a silicon substrate with a prepatterned template comprising nanoposts and nanogratings. Doing so resulted in nanoparticles that assembled in commensuration with the template design while exhibiting appreciable template-induced strain. These dense arrays of nanostructures could either be directly applied or used as lithographic masks in applications for light collection, chemical sensing, and data storage.

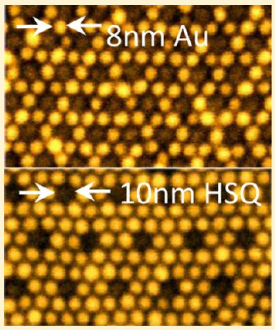


## 1. INTRODUCTION

The self-assembly of nanosized components is a promising method for nanofabrication because it provides a combination of high throughput and high resolution that extends the capability of top-down lithography, potentially surpassing the minimum feature sizes achievable by current methods. Sub-10-nm nanoparticle self-assembly has been demonstrated using Langmuir−Blodgett techniques,[1−3] drying-mediated assembly,[4] and drop-casting[5] to achieve dense arrays of 2-D nanoparticle lattices. However, existing methods are unable to control the position and orientation of these lattices or to substitute individual nanoparticles selectively with a different material. Achieving such a high degree of control would require an additional directing factor afforded by top-down lithography.

In directed self-assembly, a sparse array of structures patterned by top-down lithography is used to guide the self-assembling components that will fill in for the missing structures, thereby increasing the throughput, ordering, and density over that of each method acting in isolation. This approach has been successfully implemented in block copolymer systems with recent advances demonstrating large areas[6] and accurate control[7−9] of the resulting patterns to create different morphologies. This success could be attributed to the separability of the process of forming a block copolymer film of the desired thickness (by spin coating) from the process of forming ordered nanostructures (by annealing to induce microphase separation). To a lesser degree, directed self-assembly has also been demonstrated with particle systems, but only using microparticles and/or sparsely spaced pits or grooves with low area coverage.[10−12]

In nanoparticle systems, an analogous approach of directed self-assembly in achieving a dense coverage of sub-10-nm structures has not been reported. In part, this lack of previous work might be due to the challenges involved in creating templates with sub-10-nm feature sizes.[13] Perhaps more importantly, nanoparticles that are incompressible hard objects coated with a soft ligand shell are less mobile (as compared to block copolymer molecules) once assembled. Hence, the directed assembly of these monolayer films by allowing the nanoparticle suspension to dry onto a prepatterned template might not work because of the large degree of simultaneous nanoparticle rearrangement required. However, the spin coating of these nanoparticles onto the template might not give sufficient time for monolayer formation and rearrangement, thus resulting in disorder, missing particles, or particle aggregation.[11] This work describes a process that allows for the rearrangement of sub-10-nm particles in a preassembled monolayer and investigates the effect of varying template parameters on the resulting nanoparticle lattice. The achieved long-range ordering and controllable directionality of the nanostructures are useful in applications such as bit-patterned media,[14−16] nanophotonics,[17] and chemical sensing.[18]

## 2. EXPERIMENTAL SECTION

**2.1. Sample Preparation.** Spherical gold particles (∼8 nm core diameter) capped with oleylamine ligands (length ∼2.3 nm[19]) were synthesized according to a previously described procedure.[20] The particles were suspended in hexane and were ∼13 nm in diameter, including the ligand shell.

Templates consisting of positive relief structures (hexagonal arrays of ∼10-nm-diameter cylindrical posts as well as gratings comprising

Received: August 13, 2012
Revised: September 25, 2012
Published: September 27, 2012

  

parallel ~10-nm-wide lines) were fabricated using electron-beam lithography (EBL) based on a previously reported process.[21] In brief, hydrogen silsesquioxane resist (HSQ) was spin-coated to a thickness of 15 nm onto silicon substrates. The template structures were defined using an Elionix ELS-7000 electron-beam lithography system. The accelerating voltage and beam current were 100 kV and 500 pA, respectively. Templates were developed for 1 min in an aqueous solution of 1% NaOH and 4% NaCl, followed by rinsing under running deionized water for 1 min and blow-drying with a nitrogen gun. Experiments were performed under a nitrogen atmosphere in a glovebox.

**2.2. Process Flow of Experiment.** The process flow of our experiment is illustrated in Figure 1. The key aspect of our process is its ability to withstand organic solvents used later in the process. As a result, no further pattern transfer was needed. The template was submerged into a liquid subphase of anisole before dropwise addition of the AuNP suspension onto the liquid surface. Doing so prevented the nanoparticle film from being deposited twice onto the template (i.e., during the downward and upward strokes) and prevented excessive disruption of the particle film, which might generate defects such as cracks, voids, and multilayers. We observed that anisole provided a compatible surface on which the oleylamine-capped AuNP's could spread, possibly because of its surface tension of 29.3 mN/m, which is close to that of oleylamine (31.4 mN/m). In contrast, these nanoparticles have been observed to aggregate when assembled on water (72.8 mN/m). After the evaporation of hexane, a locally ordered monolayer film of AuNP's was formed on the surface of anisole (Figure 1b).

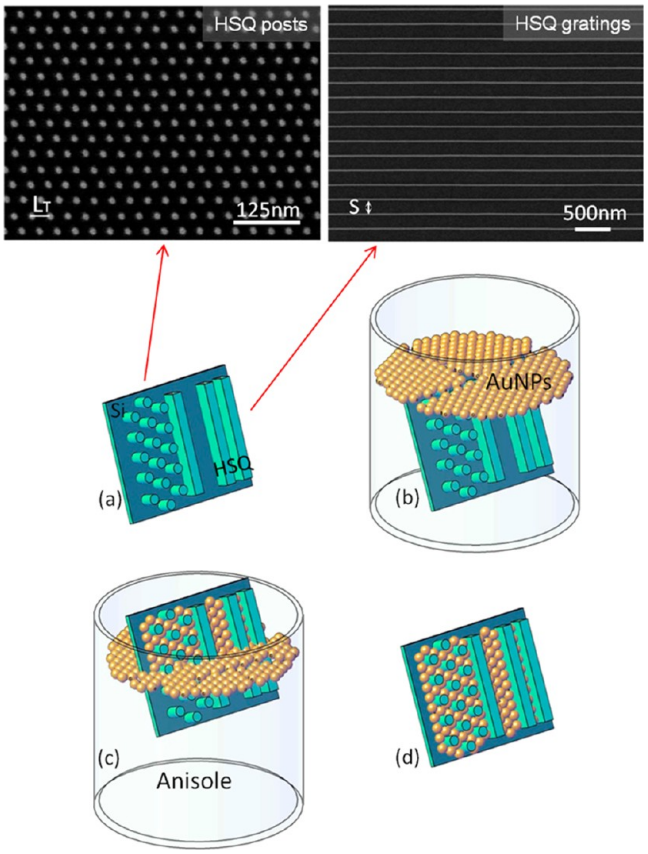


**Figure 1.** Schematic of the process used to achieve directed self-assembly of 2-D arrays of AuNP's. (a) Si substrate with an HSQ template patterned by EBL: 10-nm-diameter posts arranged in a hexagonal lattice with a lattice parameter of $L_T$ = 40 nm (top-left SEM) and 10-nm-wide gratings with a spacing of $S$ = 190 nm (top-right SEM). (b) The template is first immersed into anisole followed by the addition of a suspension of AuNP's in hexane; a locally ordered monolayer of nanoparticles forms on the surface of anisole after hexane evaporation. (c) The particle film is then deposited gradually on the template as the latter is raised out of anisole at a speed of 17 $\mu$m/s. (d) A close-packed 2-D array of AuNP's assembled according to the template design.

the separation of the monolayer-formation process from the template-directing process, where the monolayer was fed edge-wise onto the template to provide sufficient opportunity for the rearrangement of nanoparticles. The result is a dense array of ordered nanoparticles with selective substitution by the prepatterned nanostructures on the template.

Templates consisting of HSQ nanoposts and nanogratings were first fabricated[21] (Figure 1a). The main advantages of using HSQ for template-directed self-assembly were its high resolution with EBL and

The film was transferred to the template by moving the sample upward from the solution using a stepper motor at a constant speed of ~17 $\mu$m/s (Figure 1c). As the sample was removed from the solution, the AuNP's were attracted into the template patterns by capillary forces.[22,23] The template dictated the lattice orientation of the particle film, which rearranged when in close proximity to the template to form a 2-D colloidal crystal (Figure 1d). In this manner, we successfully assembled highly ordered AuNP's packed in templates.

Finally, samples were imaged in a scanning electron microscope (SEM). Image analysis was automated using codes written in ImageJ[24] and Visual Basic for Applications (Supporting Information). By comparing the lattice parameter of AuNP's within templates to their natural (unstrained) lattice parameter outside of the template, we determined the strain behavior of the AuNP assembly and its tolerance to variation in the template pitch.

## 3. RESULTS AND DISCUSSION

**3.1. Self-Assembly without a Template.** A film of nanoparticles placed on an unpatterned Si substrate showed the successful formation of a monolayer, but with only short-range ordering (Figure 2). The film was observed to consist of multiple but closely correlated orientations of hexagonally close-packed lattices[25,26] as shown in the Fourier transform inset. Gaps and connections in the monolayer appear to have formed as a result of the splitting of a continuous layer and the rearrangement of nanoparticles, respectively. This observation suggests that the attraction between nanoparticles in the

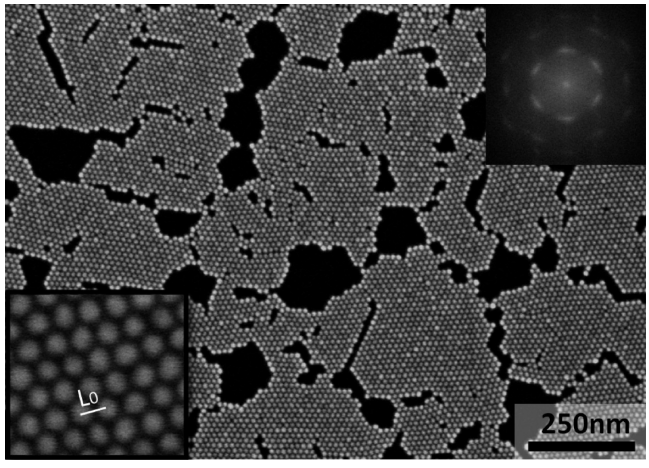


**Figure 2.** Scanning electron micrograph of AuNP's in a close-packed monolayer, showing the local ordering of the particles in the absence of a template. On average, $L_0 \approx 13$ nm is the natural pitch of the nanoparticle film. (Inset, top right) Fast Fourier transform of the SEM image, showing the presence of multiple closely correlated orientations of the hexagonal lattice.


dx.doi.org/10.1021/la303287z | *Langmuir* 2012, 28, 16782−16787

monolayer was sufficiently weak, hence allowing the dynamic detachment and reattachment of particles, which is crucial to nanoparticle rearrangement during directed self-assembly.

The natural lattice parameter of the nanoparticle film, $L_0$, was measured to be ~13(±1) nm on average (Figure 2, lower-left inset). This lattice parameter was used as the zero-strain value when analyzing nanoparticles assembled into prepatterned structures. In these instances, the template could introduce strain into the nanoparticle lattice, giving rise to either stretching or compression. We investigated these effects for both cases of nanoposts and nanogratings.

**3.2. Self-Assembly with a Template of Nanoposts.** Arrays of hexagonally arranged cylindrical nanoposts with lattice parameters, $L_T$, ranging from 26 to 40 nm (in steps of 2 nm) were used to direct the spherical nanoparticles, which naturally adopt a hexagonal close-packed lattice as well in an untemplated region (Figure 2). Figure 3a,b shows scanning electron microscope (SEM) images of template-directed self-assembly in which AuNP's are ordered in a commensurate manner within two separate nanopost lattices. The images reveal that the HSQ nanoposts (dark spots) had successfully substituted for individual nanoparticles (bright spots) in the lattice to achieve a significant degree of ordering. The orientation of the nanoparticle lattice was determined by the template. Figure 3c is an SEM image of AuNP's ordered in rows within a grating template. Defects such as double-layer formation were observed in our nanoparticle assemblies (Supporting Information Figure S3). However, the underlying layer of nanoparticles was observed to be directed by the template to form lattices of predictable orientations. To gain insight into the behavior of nanoparticles as they assemble into the templates, we focused only on regions that were not obscured by double layers.

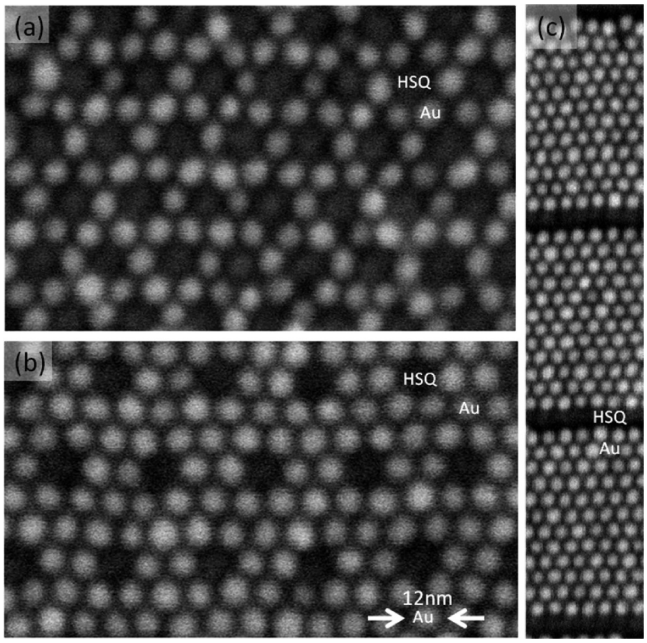


**Figure 3.** Scanning electron micrographs showing a 2-D array of AuNP's close-packed and ordered between HSQ nanoposts of (a) 26 and (b) 40 nm pitch as well as between gratings with (c) a 140 nm spacing.

To analyze the packing of nanoparticles into a template of nanoposts, we applied the concept of commensuration. For a highly ordered colloidal crystal to be formed within a template, the nanoparticle lattice must be commensurate with the nanopost lattice such that every nanopost in the template exactly substitutes for one particle in the resulting nanoparticle lattice.[7] The condition for a commensurate configuration in our system is given mathematically by the commensuration ratio $k = (L_T/L) = (i^2 + j^2 + ij)^{1/2}$, where $L$ is the lattice parameter of the nanoparticles assembled within a template that has a lattice parameter of $L_T$ and $i$ and $j$ are integers (Supporting Information). Each value of the ratio $k$ represents a commensurate configuration of the particle lattice and post lattice. The nanoparticle lattice is able to rotate, stretch, or compress to meet the commensuration condition such that the resulting lattice parameter $L \neq L_0$, where $L_0$ is the natural lattice parameter of the nanoparticles as measured outside the template. Hence, each commensurate configuration as defined by $k$ is actually valid over a range of post pitches $L_T$.

The orientation and ordering of nanoparticles for several commensurate conditions as shown in Figure 4 are described next. For integer values of $k$, the particle lattice and post lattice share the same orientation. For instance, at $k = 2$, exactly one particle fits between every two posts (Figure 3a), and at $k = 3$, exactly two particles fit between two posts (Figure 3b). However, irrational values of $k$ correspond to configurations where the particle lattice is rotated relative to the post lattice (e.g., 30° rotation with $k = 3^{1/2}$ and ±19° rotation with $k = 7^{1/2}$). The allowance for both positive and negative rotational angles results in two "degenerate" orientations as shown in the SEM images of particle assembly in a post array with $L_T = 36$ nm (Figure 4, right).

The nanoparticle lattices were observed to strain to achieve commensurability within templates. By measuring the lattice parameter of these strained lattices (Supporting Information), we experimentally obtained a range of possible strains. The maximum compressibility that was experimentally observed was ~5%, likely causing some intercalation of ligands of adjacent particles, and the maximum stretchability was ~15%. Guided by this range of allowable strain, we predicted the span of nanopost pitch, min $(L_T) < L_T <$ max $(L_T)$, within which nanoparticles are expected to fit into a given commensurate configuration. As shown in Figure 4, each commensurate configuration (open circles) was observed over a range of values of the HSQ post pitch $L_T$. At values of $L_T$ where these ranges overlapped, multiple commensurate configurations coexisted with different areal coverage within the nanopost template. In this case, the relative stability of the possible configurations is determined by the extent of deviation from their ideal post pitch (filled diamonds), with smaller deviations (i.e., lower strain) favored over larger ones. Within the nonoverlapping portion of each range, only a single commensurate configuration was observed. When $L_T$ was close to the ideal post pitch, ideal$(L_T) = kL_0$ (filled diamonds), large areas of highly ordered nanoparticle lattices could be assembled (Supporting Information Figure S3). Increasing deviation of $L_T$ from ideal$(L_T)$ at the same commensuration ratio $k$ resulted in poorer ordering, as $L$ was strained further from $L_0$. Notably, we observed total disorder at $L_T = 32$ nm, consistent with the absence of an accessible range of allowable strains at this pitch.

As can be seen in Figure 4, miniscule changes in the template lattice parameter by only 2 nm can affect the resulting commensurate orientation of the nanoparticles. Accordingly, we have limited our study to only these few commensurate


dx.doi.org/10.1021/la303287z | Langmuir 2012, 28, 16782−16787

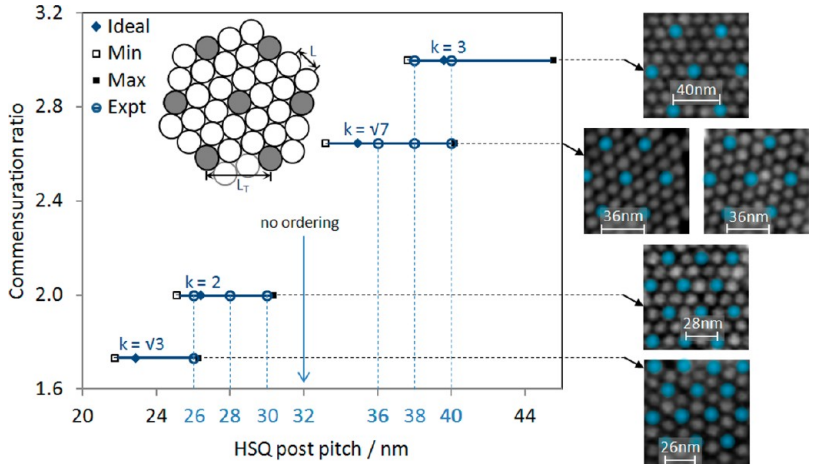


**Figure 4.** Plot of the commensuration ratio between post and particle lattices as a function of the post pitch. Experimental observations are marked with circles. (Right) SEM images of nanoparticles self-assembled in various commensurate configurations between HSQ posts of varying pitch (falsely colorized in blue for clarity). (Inset) Schematic indicating the definition of $L$ and $L_T$, showing also one possible commensurate arrangement for the case of $k = 7^{1/2}$.

orientations because increasing the template lattice parameter would make possible more commensurate orientations that compete to occupy the template region, resulting in overall poor large-area ordering.

**3.3. Self-Assembly with a Template of Nanogratings.** In grating templates, we observed the ordering of nanoparticles into rows with an average row-to-row pitch, $Y$. The number of rows that could fit between the HSQ lines depended strongly on the spacing of the lines and the strain induced in the nanoparticle lattice. We investigated the strainability of these rows of particles by comparing $Y$ with $y_0$, the "natural" row-to-row pitch of the nanoparticle film outside the template (i.e., $y_0 = L_0 \cos 30°$). The normalized strain $\varepsilon = (Y - y_0)/(y_0)$ was measured (Supporting Information) and plotted for different HSQ line spacings $S$ (also normalized by $y_0$) as shown in Figure 5. The observed strain ranged from −10 to 35%, again showing a higher tendency for the nanoparticle film to stretch than compress.

As the grating spacing increased, the nanoparticle rows would be stretched to a point where an additional row could be squeezed in, resulting in the sawtooth trend observed in Figure 5. Each segment corresponds to an integer number of rows of nanoparticles within the template, as represented by the corresponding SEM images. The overlapping of these segments (dotted rectangles) signifies that different numbers of rows were observed within the same grating spacing. In our system, these overlaps span ∼15% of $y_0$. The period of the sawtooth function is equal to the spacing increment needed to accommodate a new row. This increment is initially approximately equal to the natural row-to-row pitch $y_0$ but decreases because of the additional compression allowed by each additional row, such that subsequent rows can squeeze in before a full row pitch of $y_0$ is added. Interestingly, a similar analysis for strain along the $x$ direction (as measured for at least seven particles along the $x$ axis) did not show a correlation to grating spacing, suggesting that strain was sustained only along the $y$ axis and that the nanoparticle ligands were unable to relax the strain in the $x$ direction.

We now describe a physical model used to obtain the trend lines that were used to fit the data in Figure 5. In this model, we focus not on the number of nanoparticle rows ($N$) but on the number of inter-row gaps occupied by the ligands ($N + 1$) that

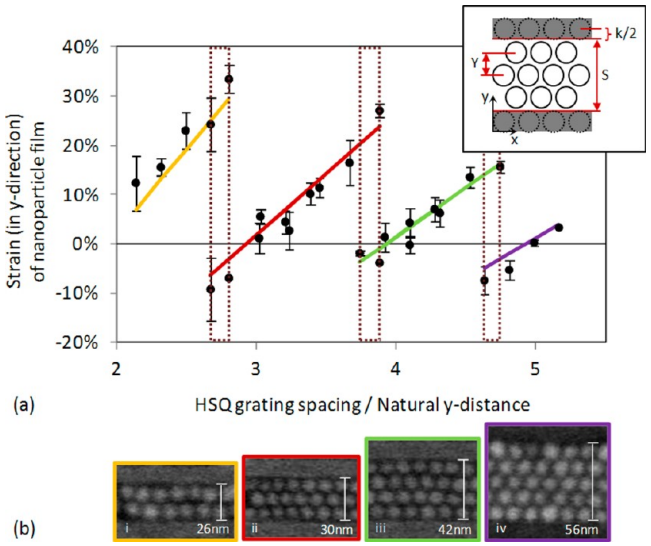


**Figure 5.** (a) Plot of the average strain between rows of particles, $\varepsilon$, as a function of the normalized spacing between the HSQ gratings. The average row-to-row pitch in an untemplated region, $y_0$, is taken as the natural row-to-row pitch of the particles. The normalized spacing ($S/y_0$) is approximately equal to the number of particle rows, $N$, that can fit into a grating spacing of $S$ at zero strain ($\varepsilon = 0$). Strain is calculated as $\varepsilon = (Y - y_0)/(y_0)$, where $Y$ is the average row-to-row pitch of the particles in the template. Error bars show the standard deviation of $Y$ at each grating spacing. Fit lines are obtained using the model equation $Y = (S + k)/(N + 1)$, where $k$ is a constant. (b) Representative SEM images of nanoparticles self-assembled in rows between HSQ gratings.

can fit between the HSQ lines. When the rows of nanoparticles are stretched by $\Delta S$, the total strain is distributed among these $N + 1$ rows of ligands, resulting in a strain of $\Delta Y = (\Delta S)/(N + 1)$ per row. Thus, the slope of segments in Figure 5 is given by $(1)/(N + 1)$. We calculated theoretical values of the average row-to-row pitch $Y$ from the model equation $Y = (S + k)/(N + 1)$ and input these values into the strain equation $\varepsilon = (Y - y_0)/(y_0)$ to obtain trend lines that fit each set of data points in Figure 5. Here, $Y$ is the theoretical row-to-row pitch and $k$ is a fitting parameter with a value of ∼11 nm, where $k/2$ has physical meaning for the average distance from the HSQ line edge to


dx.doi.org/10.1021/la303287z | Langmuir 2012, 28, 16782−16787

the center of a row of imaginary particles for which the HSQ line substitutes (schematic in Figure 5 inset).

## 4. CONCLUSIONS

Our experimental results show that the ordering of monodisperse particles in a template was directly controlled by the pattern geometry and the dimensions of the template. Remarkably, the ordering behavior of nanoparticles in both nanopost and grating templates was observed to be analogous to commensuration in the drastically different system of block copolymers,[7] underlining the thermodynamics (i.e., the minimization of free energy) governing self-assembling systems. Given the high speed at which the assembly front advances (17 $\mu$m/s), the ability of the nanoparticles to rearrange and be directed by the template suggests a high degree of nanoparticle mobility.

In the case of the nanopost template, the nanoparticle lattice orientation was observed to be sensitive to 2 nm steps in the template lattice parameter. This nanometer precision required in template fabrication is a potential issue in directing the self-assembly of sub-10-nm particles and highlights a challenge in achieving large-area ordering. For instance, a jitter in nanopost position introduced during the lithography process could induce local regions of varying lattice parameters.[27] However, grating templates provide an alternative that allows a greater degree of tolerance for error in the lithography process. The observation that nanoparticles do not land on top of nanoposts or grating lines suggests that the ordering of nanoparticles is driven by capillary forces where a meniscus of the liquid subphase is subtended by the patterned nanostructures.

In summary, the templating scheme affects the ordering and strain of the nanoparticle lattice. Templates consisting of nanopost arrays afford greater control of the positioning, directionality, and ordering of the particle film. However, templates consisting of gratings achieve a larger range of strain tolerance (−10 to 35%) at the expense of substituting for entire rows of particles and cannot control the position of particles along the $x$ direction.

In conclusion, we have directed the self-assembly of sub-10-nm gold nanoparticles into dense arrays of nanostructures, which is useful for nanophotonics, chemical sensing, and data storage applications. By collecting a preassembled monolayer of nanoparticles edgewise onto a lithographically patterned template, the particles approaching the template surface are thought to rearrange to fit in a commensurate manner with the template. Extensive image analysis of ordered arrays shows that the nanoparticle lattice would preferentially stretch rather than compress to assemble within the template. The assembly of nanoparticles of other materials and shapes would be possible with this approach. Future work will focus on improving large-area ordering by controlling the monodispersity of nanoparticles and controlling the surface pressure of the monolayer in a Langmuir−Blodgett trough.

## ■ ASSOCIATED CONTENT

### Supporting Information

Image analysis details, discussion of commensuration, and additional SEM images. This material is available free of charge via the Internet at http://pubs.acs.org.

## ■ AUTHOR INFORMATION

### Corresponding Author

*E-mail: yangkwj@imre.a-star.edu.sg.

### Notes

The authors declare no competing financial interest.

## ■ ACKNOWLEDGMENTS

This work was supported by the Agency for Science, Technology and Research (A*STAR) in Singapore. The work made use of the SERC nano Fabrication, Processing and Characterization (SnFPC) facilities in IMRE. We acknowledge K. Kumar (IMRE) for fruitful discussions.

## ■ REFERENCES

(1) Chen, X.; Lenhert, S.; Hirtz, M.; Lu, N.; Fuchs, H.; Chi, L. Langmuir-Blodgett patterning: a bottom-up way to build mesostructures over large areas. *Acc. Chem. Res.* **2007**, *40*, 393−401.

(2) Park, Y.-K.; Yoo, S.-H.; Park, S. Assembly of highly ordered nanoparticle monolayers at a water/hexane interface. *Langmuir* **2007**, *23*, 10505−10510.

(3) Isa, L.; Kumar, K.; Muller, M.; Grolig, J.; Textor, M.; Reimhult, E. Particle lithography from colloidal self-assembly at liquid-liquid interfaces. *ACS Nano* **2010**, *4*, 5665−5670.

(4) Ku, J.; Aruguete, D. M.; Alivisatos, A. P.; Geissler, P. L. Self-assembly of magnetic nanoparticles in evaporating solution. *J. Am. Chem. Soc.* **2011**, *133*, 838−848.

(5) Bigioni, T. P.; Lin, X. M.; Nguyen, T. T.; Corwin, E. I.; Witten, T. A.; Jaeger, H. M. Kinetically driven self assembly of highly ordered nanoparticle monolayers. *Nat. Mater.* **2006**, *5*, 265−270.

(6) Ruiz, R.; Kang, H.; Detcheverry, F. A.; Dobisz, E.; Kercher, D. S.; Albrecht, T. R.; de Pablo, J. J.; Nealey, P. F. Density multiplication and improved lithography by directed block copolymer assembly. *Science* **2008**, *321*, 936−939.

(7) Bita, I.; Yang, J. K. W.; Jung, Y. S.; Ross, C. A.; Thomas, E. L.; Berggren, K. K. Graphoepitaxy of self-assembled block copolymers on two-dimensional periodic patterned templates. *Science* **2008**, *321*, 939−943.

(8) Yang, J. K. W.; Jung, Y. S.; Chang, J.-B.; Mickiewicz, R. A.; Alexander-Katz, A.; Ross, C. A.; Berggren, K. K. Complex self-assembled patterns using sparse commensurate templates with locally varying motifs. *Nat. Nanotechnol.* **2010**, *5*, 256−260.

(9) Cheng, J. Y.; Mayes, A. M.; Ross, C. A. Nanostructure engineering by templated self-assembly of block copolymers. *Nat. Mater.* **2004**, *3*, 823−828.

(10) Xia, Y.; Yin, Y.; Lu, Y.; McLellan, J. Template-assisted self-assembly of spherical colloids into complex and controllable structures. *Adv. Funct. Mater.* **2003**, *13*, 907−918.

(11) Dai, Q.; Rettner, C. T.; Davis, B.; Cheng, J.; Nelson, A. Topographically directed self-assembly of goldnanoparticles. *J. Mater. Chem.* **2011**, *21*, 16863−16865.

(12) Badini-Confalonieri, G. A.; Vega, V.; Ebbing, A.; Mishra, D.; Szary, P.; Prida, V. M.; Petracic, O.; Zabel, H. Template-assisted self-assembly of individual and clusters of magnetic nanoparticles. *Nanotechnology* **2011**, *22*, 285608.

(13) Leu, J. C. Templated Self-Assembly of sub-10 nm Quantum Dots. M.Sc. Dissertation, Massachusetts Institute of Technology, Cambridge, MA, 2008.

(14) Albrecht, M.; Hu, G.; Guhr, I. L.; Ulbrich, T. C.; Boneberg, J.; Leiderer, P.; Schatz, G. Magnetic multilayers on nanospheres. *Nat. Mater.* **2005**, *4*, 203−206.

(15) Asbahi, M.; Moritz, J.; Dieny, B.; Gourgon, C.; Perret, C.; van de Veerdonk, R. J. M. Recording performances in perpendicular magnetic patterned media. *J. Phys. D: Appl. Phys.* **2010**, *43*, 385003.

(16) Yang, J. K. W.; Chen, Y.; Huang, T.; Duan, H.; Thiyagarajah, N.; Hui, K. H.; Leong, S. H.; Ng, V. Fabrication and characterization of bit-patterned media beyond 1.5 Tbit/in$^2$. *Nanotechnology* **2011**, *22*, 385301.

(17) Bohn, J.; Ben-Moshe, M.; Tikhonov, A.; Qu, D.; Lamont, D.; Asher, S. A. Charge stabilized crystalline colloidal arrays as templates for fabrication of non-close-packed inverted photonic crystals. *J. Colloid Interface Sci.* **2010**, *344*, 298−307.

(18) Fan, J. A.; Wu, C.; Bao, K.; Bao, J.; Bardhan, R.; Halas, N. J.; Manoharan, V. N.; Nordlander, P.; Shvets, G.; Capasso, F. Self-assembled plasmonic nanoparticle clusters. *Science* **2010**, *328*, 1135−1138.
(19) Compton, O. C.; Osterloh, F. E. Evolution of size and shape in the colloidal crystallization of gold nanoparticles. *J. Am. Chem. Soc.* **2007**, *129*, 7793−7798.
(20) Lau, C. Y.; Duan, H.; Wang, F.; He, C. B.; Low, H. Y.; Yang, J. K. W. Enhanced ordering in gold nanoparticles self-assembly through excess free ligands. *Langmuir* **2011**, *27*, 3355−3360.
(21) Yang, J. K. W.; Berggren, K. K. Using high-contrast salty development of hydrogen silsesquioxane for sub-10-nm half-pitch lithography. *J. Vac. Sci. Technol., B* **2007**, *25*, 2025−2029.
(22) Kralchevsky, P. A.; Nagayama, K. *Particles at Fluid Interfaces and Membranes*; Elsevier: Amsterdam, 2001.
(23) Binks, B. P.; Horozov, T. S. *Colloidal Particles at Liquid Interfaces*; Cambridge University Press: Cambridge, England, 2006.
(24) Rasband, W. S. *ImageJ*; U.S. National Institutes of Health: Bethesda, MD, http://imagej.nih.gov/ij/.
(25) Wen, T.; Majetich, S. A. Ultra-large-area self-assembled monolayers of nanoparticles. *ACS Nano* **2011**, *5*, 8868−8876.
(26) Williams, D. E. G. Packing fraction of a disk assembly randomly close packed on a plane. *Phys. Rev. E* **1998**, *57*, 7344−7345.
(27) Mickiewicz, R. A.; Yang, J. K. W.; Hannon, A. F.; Jung, Y.-S.; Alexander-Katz, A.; Berggren, K. K.; Ross, C. A. Enhancing the potential of block copolymer lithography with polymer self-consistent field theory simulations. *Macromolecules* **2010**, *43*, 8290−8295.